Liu et al. *Zool. Res.* 2023, 44(1): 153−168
https://doi.org/10.24272/j.issn.2095-8137.2022.254

ZR | Zoological Research

Article Open Access

Defects and asymmetries in the visual pathway of non-human primates with natural strabismus and amblyopia

Feng Liu[1,#], Zhong-Hao Wang[1,#], Wanjing Huang[1,#], Ying Xu[2], Xuan Sang[1], Ruifeng Liu[1], Zhou-Yue Li[1], Ya-Lan Bi[3], Lei Tang[1], Jing-Yi Peng[1], Jia-Ru Wei[1], Zhi-Chao Miao[3,4], Jian-Hua Yan[1,*], Sheng Liu[1,5,*]

[1] *State Key Laboratory of Ophthalmology*, *Zhongshan Ophthalmic Center*, *Sun Yat-Sen University*, *Guangdong Provincial Key Laboratory of Ophthalmology and Visual Science*, *Guangzhou*, *Guangdong* 510060, *China*

[2] *Guangdong-Hongkong-Macau Institute of CNS Regeneration*, *Jinan University*, *Guangzhou*, *Guangdong* 510632, *China*

[3] *European Molecular Biology Laboratory*, *European Bioinformatics Institute (EMBL-EBI)*, *Wellcome Genome Campus*, *Cambridge CB10 1SD*, *UK*

[4] *Translational Research Institute of Brain and Brain-Like Intelligence and Department of Anesthesiology*, *Shanghai Fourth People's Hospital Affiliated to Tongji University School of Medicine*, *Shanghai* 200081, *China*

[5] *Guangdong Province Key Laboratory of Brain Function and Disease*, *Guangzhou*, *Guangdong* 510080, *China*

ABSTRACT

Strabismus and amblyopia are common ophthalmologic developmental diseases caused by abnormal visual experiences. However, the underlying pathogenesis and visual defects are still not fully understood. Most studies have used experimental interference to establish disease-associated animal models, while ignoring the natural pathophysiological mechanisms. This study was designed to investigate whether natural strabismus and amblyopia are associated with abnormal neurological defects. We screened one natural strabismic monkey (*Macaca fascicularis*) and one natural amblyopic monkey from hundreds of monkeys, and retrospectively analyzed one human strabismus case. Neuroimaging, behavioral, neurophysiological, neurostructural, and genovariation features were systematically evaluated using magnetic resonance imaging (MRI), behavioral tasks, flash visual evoked potentials (FVEP), electroretinogram (ERG), optical coherence tomography (OCT), and whole-genome sequencing (WGS), respectively. Results showed that the strabismic patient and natural strabismic and amblyopic monkeys exhibited similar abnormal asymmetries in brain structure, i.e., ipsilateral impaired right hemisphere. Visual behavior, visual function, retinal structure, and fundus of the monkeys were impaired. Aberrant asymmetry in binocular visual function and structure between the strabismic and amblyopic monkeys was closely related, with greater impairment of the left visual pathway.

Received: 25 October 2022; Accepted: 05 December 2022; Online: 06 December 2022

Foundation items: This study was supported by the National Natural Science Foundation of China (81870682, 81961128021, 81670885), National Key R&D Program of China (2022YEF0203200, 2021ZD0200103, 2018YFA0108300), Guangdong Provincial Key R&D Programs (2018B030335001, 2018B030337001), Local Innovative and Research Teams Project of Guangdong (2017BT01S138), and Science and Technology Program of Guangzhou (202007030011, 202007030010)

[#]Authors contributed equally to this work

*Corresponding authors, E-mail: yanjh2011@126.com; liush87@mail.sysu.edu.cn

Several similar known mutant genes for strabismus and amblyopia were also identified. In conclusion, natural strabismus and amblyopia are accompanied by abnormal asymmetries of the visual system, especially visual neurophysiological and neurostructural defects. Our results suggest that future therapeutic and mechanistic studies should consider defects and asymmetries throughout the entire visual system.

Keywords: Non-human primates; Natural disease models; Strabismic patients; Strabismus; Amblyopia

INTRODUCTION

Macaques (genus *Macaca*) diverged from the ancestors of humans and apes 25 million years ago and share highly conserved protein sequences and >90% of DNA sequence similarity with humans (Picaud et al., 2019). Macaques are highly relevant and valuable models for human ophthalmological research due to their distinctive human-like attributes, including trichromatic vision, macula structure, binocular convergence, and forward-facing eyes with overlapping visual fields. Similar to humans, macaques also have susceptibility genes for age-related macular degeneration, as well as genotype-phenotype correlations for certain inherited retinal diseases such as retinitis pigmentosa (Ikeda et al., 2018) and achromatopsia (Moshiri et al., 2019). Furthermore, macaques have been used to model and develop treatments for many complex ophthalmic diseases, such as diabetic retinopathy, choroidal neovascularization, glaucoma (Burgoyne, 2015; Lambert et al., 2019), and wet age-related macular degeneration (Lebherz et al., 2005; MacLachlan et al., 2011). Nevertheless, due to the low incidence of spontaneous ocular disease, with only a few animals affected even in the largest research colonies, the underlying pathogenesis and associated triggers have long been overlooked.

Strabismus and amblyopia are common neurodevelopmental ophthalmic diseases caused by abnormal visual experiences during the sensitive period of nervous system development. These diseases affect 2%–4% of children worldwide (Greenberg et al., 2007; Joly & Frankó, 2014). Strabismus is characterized by misalignment of the eyes, and amblyopia is clinically defined as deficits in visual acuity, contrast sensitivity, stereoscopic depth perception, and ocular motility (Mendola et al., 2018). Importantly, strabismus causes visual defects during development, such as amblyopia and loss of binocular vision, leading to loss of stereopsis and poor performance of many practical tasks that require accurate judgment of depth or distance (Ye et al., 2014). Amblyopia, typically secondary to strabismus, also affects the development of a broad range of neural, sensory, oculomotor, and perceptual functions of vision (Levi, 2012; Wong et al., 2005). As strabismus is the most common risk factor for amblyopia (Gopal et al., 2019), any causal relationship between strabismus and amblyopia is likely to be strongly related. Strabismus and amblyopia always occur during critical periods of nervous system development and may result from organic pathology of the visual pathway, visual deprivation, or functional abnormalities. Generally, early abnormal visual experience disrupts interocular alignment, resulting in strabismus, and interferes with sensory development, leading to amblyopia (Smith III et al., 2017). Previous studies have reported that strabismus disrupts binocular synaptic integration in the primary visual cortex (Scholl et al., 2013) and any anatomo-functional abnormality within the visual cortex can lead to strabismus (Quoc & Milleret, 2014). Abnormal functional properties of neurons and neuronal maps of the primary visual area and visual areas from the dorsal and ventral streams have also been observed (Quoc & Milleret, 2014; Wong, 2012). Similarly, morphological and functional changes in the visual cortex and lateral geniculate nucleus are associated with various types of amblyopia (Liao et al., 2019; Zhang et al., 2021). However, the exact pathogenesis of strabismus and amblyopia is still not fully understood.

At present, our understanding of these complex neurodevelopmental diseases is limited by our ability to appreciate neurological abnormalities, especially in the visual pathway. Although considerable efforts have been expended to develop disease-associated animal models using experimental interference, none can fully mimic the natural pathophysiology of these diseases. Therefore, investigations involving laboratory animals, particularly natural diseases in non-human primates (NHPs), are crucial. In addition, current treatment options, especially surgical correction, fail to adequately address the root cause of strabismus and amblyopia, leading to recurrence. Therefore, understanding the nature of strabismus and amblyopia and their relationship is critical for developing the most effective management strategies for these visual system defects.

Given these previously underappreciated complexities, little is known about the visual defects associated with natural strabismus and amblyopia, especially direct alterations in the visual pathway. To investigate the underlying pathogenesis and corresponding visual system defects of natural strabismus and correlative amblyopia, we screened a natural strabismic monkey and a natural amblyopic monkey from hundreds of monkeys, as well as a matched human case of clinical strabismus. Notably, we identified several visual defects and asymmetries from the retina to the visual cortex in the natural strabismic and amblyopic monkeys, suggesting the importance of evaluating overall visual system defects and asymmetries in future clinical treatments and mechanistic research related to strabismus and amblyopia.

MATERIALS AND METHODS

Retrospective case of clinical strabismus

The medical records, clinical diagnosis, and magnetic resonance imaging (MRI) scans of a recent strabismic patient (Chinese, female, 22 years old) with an established diagnosis of alternating concomitant exotropia were analyzed retrospectively. The patient was seen at the Strabismus Amblyopia Specialty of Zhongshan Ophthalmic Center, Sun Yat-Sen University, China. The following preoperative

characteristics were collected from medical records: name, sex, unique Chinese identity number, age at operation, medical history, deviation and motility of eyeballs, fixation, and binocular vision. This study was approved by the Medical Ethics Committee of Zhongshan Ophthalmic Center (approval No. 2022KYPJ004), and corresponding informed consent was obtained from the patient.

NHPs and rearing paradigms

One natural strabismic monkey (*M. fascicularis*, male, 4 years old, 3 kg) and one natural amblyopic monkey (*M. fascicularis*, male, 1 year old, 1 kg) were screened from 300 monkeys at Guangdong Chunsheng Biotechnology Development Co. (China) and confirmed by clinical diagnosis (Figure 1). A matched normal adult monkey was chosen as a control group. The clinical symptoms of natural strabismus in the monkey were similar to those of the strabismic patient. The monkeys were subsequently reared at the Experimental Animal Center of Zhongshan Ophthalmic Center until reaching adulthood and their comprehensive features were further investigated. The facility room was maintained under a 12 h:12 h light-dark cycle at 26 ℃ and 40%–60% relative humidity. Monkeys had *ad libitum* access to water and were fed a standard primate chow supplemented with fresh fruit and nuts daily. Except for the behavioral tasks, the monkeys were anesthetized by an intramuscular injection of modest Zoletil® 50 (4 mg/kg, Virbac group, France) and xylazine hydrochloride (0.2 mg/kg, Dunhua Shengda Animal Medicine, China) followed by subcutaneous injection of atropine sulphate (0.04 mg/kg, Henan Runhong Pharmaceutical, China). Both eyes were dilated using tropicamide (1%) and phenylephrine hydrochloride (2.5%, Shenyang Sinqi Pharmaceutical, China). All studies were approved by the Animal Ethics Committee of Zhongshan Ophthalmic Center (approval No. 2019-039) and complied with the ARVO Guidelines for the Use of Animals in Ophthalmic and Vision Research.

MRI

Neuroimaging analysis was first conducted to identify gross anatomical abnormalities in the whole brains of monkeys. High-resolution images were acquired using a Siemens Skyra 3.0 T (Siemens Healthcare GMbH, Germany). Before scanning, the anesthetized monkeys were placed onto the coil bed with heads fixed. Body temperature was maintained using padding for thermal insulation. During the session, whole brain volumes were obtained, and the horizontal plane was reconstructed offline using syngo fastView software (Siemens AG, Germany).

Behavioral tasks and data analysis

All monkeys were behaviorally trained several times in standard breeding environments prior to their participation in the tasks. We used conventional fruit inducement to provide the monkeys with the motivation to perform behavioral tasks and to evaluate their visual behavioral abilities. The protocols (i.e., fruits+no-hiding, fruits+hiding, and no-fruits+no-hiding) were systematically assessed to determine visual behavior differences. To avoid the impact of memory, the exact position of the reward was semi-random. Monkey behavior was constantly monitored using a video camera placed in front of the cage. Detection time was defined as the period from giving the reward until the end of the foraging state. Palm moving trajectory and detection time were determined and analyzed using Matlab software (R2021a; MathWorks, Inc., USA).

Flash visual evoked potential (FVEP), electroretinogram (ERG), and data analyses

FVEP recordings to a brief white flash (1 Hz) were applied using the RETI-scan system (Roland Consult, Germany). Recording, reference, and ground electrodes were placed on the occipital scalp, frontal scalp, and parietal scalp of the anesthetized monkeys, respectively (Odom et al., 2016). The eyes were protected using 2.5% hypromellose gel (Shanghai Sine Pharmaceutical Laboratories, China) to maintain corneal hydration. During FVEP and ERG recording sessions, the impedances of each recording and reference electrodes for both eyes were maintained at the same value and at less than 4 kΩ. Body temperature was maintained at 36–38 °C with a water-circulation heating pad. Monocular stimulation was performed with a shield covering the other unstimulated eye.

ERG responses were acquired using standard gold-plated cup electrodes, as described previously (Liu et al., 2018). Briefly, recording, reference, and ground electrodes were held in the center of the cornea, external canthus, and forehead, respectively. The following recording session procedures were performed: (1) scotopic threshold response (STR, retinal ganglion cells, RGCs), (2) scotopic rod response (only rod), (3) scotopic maximal response (mixed rod-cone), (4) photopic negative response (PHNR, RGCs), (5) photopic response (cone), (6) 10 Hz flicker response (ON cone), and (7) 30 Hz flicker response (OFF cone). The scotopic ERG responses to different light intensities were first recorded after 60 mins of dark adaptation. During the scotopic course, white flash luminances of 0.00028, 0.0092, and 2.9 cd·s/m^2 were used to induce STR (Fortune et al., 2004), rod response (Marmor et al., 2009), and mixed rod-cone response, respectively. The eyes were then adapted to blue background light for 10 mins, and PHNR was elicited by red flash stimulation (Rangaswamy et al., 2007). For the following photopic steps, a steady white background-adapting field was presented to saturate the rod system. Full-field white flash stimuli of 2.9 cd·s/m^2 at 10 Hz and 30 Hz were also applied for the flicker ERG recordings.

ERG waveforms were analyzed after applying 50 Hz low-pass filtering, except for scotopic oscillatory potentials (OPs), which were subjected to 75–300 Hz band-pass filtering. For FVEP, latency was measured as the duration from stimulus onset to the N2 trough, and the corresponding amplitude was calculated from the preceding N2 trough to the P2 peak. For scotopic and photopic analyses (Liu et al., 2021, 2018), the a-wave amplitude, reflecting the activity of photoreceptors, was calculated from the baseline to the first trough. The b-wave amplitude, reflecting the function of bipolar cells, was calculated from the first trough to the following peak. Related latencies were defined from the stimulus onset to the first trough and the following peak. For OPs, the amplitude and latency of the wavelet with the maximum response were measured. For PHNR, the amplitude of the negative trough following the b-wave was defined from the baseline to the trough, and its latency was also measured accordingly. For

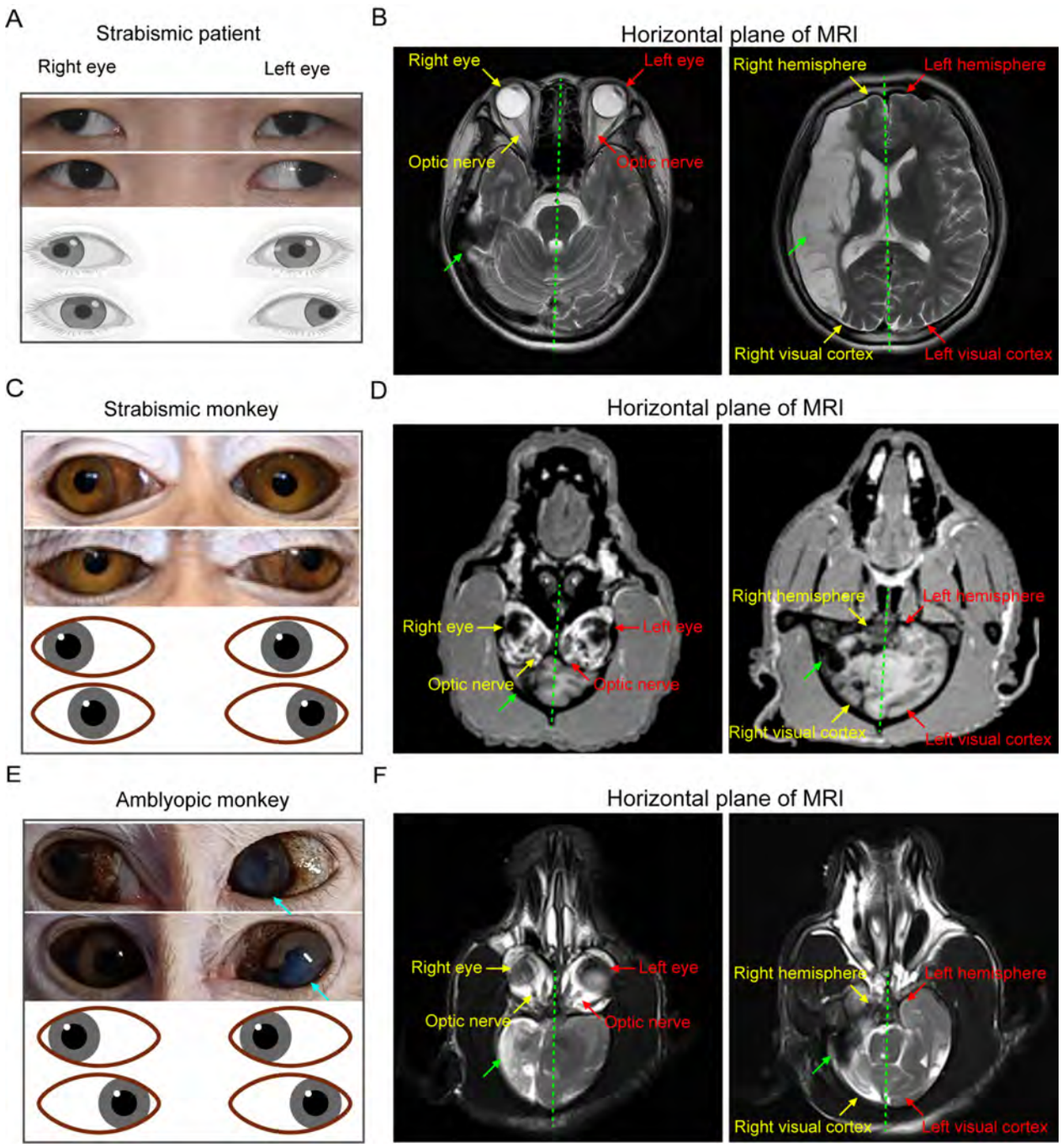

Figure 1 Strabismic patient and natural strabismic and amblyopic monkeys all exhibit aberrant asymmetrical impairment of the brain structure

A, C, E: Representative eye movement images (top) and corresponding models (bottom) of strabismic patient (A) and natural strabismic (C) and amblyopic (E) monkeys. Natural strabismic and amblyopic monkeys were screened from hundreds of monkeys using ophthalmic clinical diagnosis. Strabismic patient and monkey showed ocular symptoms of alternating concomitant exotropia, whereas natural amblyopic monkey had normal eye movements but with leukoma and partial iris abnormality in the left eye. B, D, F: Horizontal plane view of whole brain volumes of strabismic patient (B) and natural strabismic (D) and amblyopic (F) monkeys, scanned by MRI. Right hemisphere of strabismic patient (B) showed abnormal asymmetrical ischemic impairment, especially in the visual cortex. Brain structural development in natural strabismic (D) and amblyopic (F) monkeys also exhibited some aberrant asymmetries, particularly atrophic visual cortex in the smaller right hemisphere. General structures of both eyes and optic nerves looked very similar. Red, yellow, and green arrows represent left, right, and abnormal part of the brain structure, respectively. Cyan arrows represent leukoma and partial iris abnormality in left eye of amblyopic monkey. Green dotted line indicates central line of whole brain. MRI, magnetic resonance imaging.

flickers, the trough-to-peak amplitude of the wavelet with the maximum response was measured, and its latency was calculated from stimulus onset to the first peak.

Optical coherence tomography (OCT) and data analysis

An ultra-high resolution OCT system (Spectralis; Heidelberg Engineering GmbH, Germany) was applied to identify and estimate the thickness of different retinal layers. Each anesthetized monkey was placed on a platform in front of the camera lens and retinas were scanned by OCT. The scan consisted of 31 lines, with the fovea scan taken along the central line of the fovea. For analysis, OCT images were subjected to contrast enhancement using scripts in Matlab. To obtain precise segmentation, nine segmentations were performed quantitatively and semi-automatically by manually selecting the boundary between two adjacent layers (Figure 5A). After reconstructing the 3D view of all retinal layers, each layer data point from the 31 lines scanned along the fovea center was averaged. The fovea thickness curve was drawn using the boundary points of the fovea scan, and the mean thickness curve was obtained by fitting and calculating the average boundary point of the 31 scan lines. The fitting area-to-length ratio was then used to calculate mean thickness between two adjacent retinal layers. The analysis codes used are available at the GitHub repository: https://github.com/LFVZYM/ShengLiuLab. The mean thicknesses of both retinas, as well as the fovea scan thickness, were compared among the normal, strabismic, and amblyopic monkeys. We also reconstructed the central fovea structures and evaluated their differences in area, height, maximum width, diameter, and full-width half-maximum (FWHM). Additionally, fundus images of the normal, strabismic, and amblyopic monkeys were also acquired, and the cup-to-disc ratio (CDR) was calculated as the diameter proportion between the optic cup and optic disc. For functional and structural asymmetrical analysis of the natural strabismic and amblyopic monkeys, the left-to-right side ratio (L/R ratio) was used to assess differences in FVEP and PHNR amplitude, brain hemispherical area, ganglion cell layer (GCL) thickness, etc. Functional and structural correlations and statistical analyses were performed with GraphPad Prism software (v9.0, Dotmatics, USA).

Whole-genome sequencing (WGS) and bioinformatics analysis

Blood samples were obtained from the strabismic and amblyopic monkeys and tested to determine adequate concentration and quality for DNA degradation and purity before WGS. Target DNA was prepared and sequencing was performed using the NovaSeq 6000 system (Illumina, USA) with 2×150 bp paired-end reads. After sequencing, bioinformatics analysis was executed using Burrows-Wheeler Aligner, SAMtools, VCFtools, SnpEff, etc. In brief, Burrows-Wheeler Aligner was employed to map reads to the *M. fascicularis* reference genome (6.0). SnpEff was used to annotate and predict the effects of genetic variants, namely high, moderate, low, and modifiers (Cingolani et al., 2012). Considering the degree of protein disruption, only “impactful” variants, identified by high and moderate effects, were used for further analysis. To detect potential hereditary disease driver genes, we performed text mining of gene-disease associations using the DisGeNET discovery platform (https://www.disgenet.org/search). DisGeNET integrates information on diseases and genes from expert-curated databases and scientific literature using text-mining approaches (Piñero et al., 2015). To facilitate variant interpretation, candidate genes were further mapped, and target gene interaction networks were constructed using the String database and Cytoscape software (v3.8.0, National Resource for Network Biology, USA).

RESULTS

Strabismic patient and natural strabismic and amblyopic monkeys show abnormal asymmetrical brain structures

To better understand the underlying visual defects of natural strabismus and correlative amblyopia, we first retrospectively analyzed a human clinical case of strabismus. The strabismic patient was clinically diagnosed with concomitant alternating exotropia with normal extraocular muscles (Figure 1A). The central sight of both eyes deviated outward alternately and failed to fix on an object simultaneously. To explore possible neurological abnormalities, MRI analysis revealed an abnormal asymmetrical volume of the whole brain between the left and right hemispheres (Figure 1B; Supplementary Figure S1A), especially an impaired visual cortex in the right hemisphere. Notably, the right hemisphere showed extensive aberrant damage, and overall symmetry of the whole brain structure was reduced.

To investigate the underlying pathogenesis of the natural diseases and corresponding visual system defects, NHPs were employed to simulate the same distinctive human visual attributes. We successfully screened one natural strabismic monkey (Figure 1C) and one natural amblyopic monkey (Figure 1E) from hundreds of monkeys and evaluated their neurostructural, behavioral, neurophysiological, and genetic changes. As shown in Figure 1C, the clinical features of the natural strabismic monkey with normal extraocular muscles also included alternating outward deviation of the eyes, consistent with the ocular features of the concomitant strabismic patient (Figure 1A). Although the natural amblyopic monkey could simultaneously focus on an interesting object, the left eye showed corneal leukoma and partial iris abnormality (Figure 1E). Intraocular pressure was within the normal range for the strabismic patient and all monkeys, indicating the absence of overt glaucomatous ocular hypertension. To link the natural monkeys and strabismic patient, we also investigated anatomical differences between the left and right brain hemispheres using representative MRI images scanned from the horizontal plane, as shown in Figure 1D, F and Supplementary Figure S1B, C. While the anatomical structures of the eye and optic nerve looked similar between the left and right sides, whole brains of the natural strabismic and amblyopic monkeys also exhibited many similar abnormal asymmetrical structures, especially in the smaller right hemisphere. The visual cortex volume in the right hemisphere was smaller than that in the left hemisphere,

suggesting a weaker role for the atrophied right visual cortex in the left visual pathway. Part of the left hemisphere volume also extended to the right side of the brain. Notably, the strabismic monkey appeared to have a more severe degree of brain structure abnormalities than the amblyopic monkey. Taken together, these data suggest that abnormal asymmetrical brain impairment may be the main cause of strabismus and amblyopia.

Natural strabismic and amblyopic monkeys show weaker visual behavioral ability

As the brain anatomy of the natural strabismic and amblyopic monkeys was asymmetrical and associated with the visual pathways, we next compared the visual behavioral ability of the monkeys to one matched normal adult monkey using three reward-inducing behavioral tasks, i.e., fruits+no-hiding, fruits+hiding, and no-fruits+no-hiding (Figure 2). For the normal monkey shown in Figure 2A, B, D, and F (left), the moving trajectory was relatively simple and the motivation to gain the random reward was more targeted and tenacious. In contrast, the natural strabismic monkey showed a more complex moving trajectory, with a larger range of motion around the reward (Figure 2B, D, middle). The strabismic monkey also showed poorer accuracy at targeting the random reward, with its hand always deviating away (Figure 2A, middle). In the no-fruits+no-hiding protocol, the strabismic monkey was more likely to explore for the non-existing reward (Figure 2F, middle). The natural amblyopic monkey was very timid and often stayed in the corner with no sufficient motivation to explore for the random reward (Figure 2A, F, right). The amblyopic monkey spent more than 5 mins without identifying the fixed reward position in the fruits+hiding protocol (Figure 2D, right). Quantitative results showed that the detection times of the strabismic monkey for the three tasks were longer than those of the normal monkey, as well as the amblyopic monkey in the fruits+no-hiding and fruits+hiding protocols (Figure 2C, E, G). Thus, the natural strabismic and amblyopic monkeys exhibited weaker visual behavioral abilities, suggesting that these disorders disrupted visual perception.

Natural strabismic and amblyopic monkeys show weaker visual function

Given the poorer visual behavior of the impaired monkeys, we further investigated visual neurophysiological defects using FVEP and ERG recordings. We first assessed functional differences in retinal inner neurons, especially RGCs. FVEP analysis can be used to quantify the functional integrity of the visual pathway, including RGCs, optic nerves, and the visual cortex (Odom et al., 2016). Based on the FVEP results, the visual functional latencies were longer, but the amplitudes were lower in the strabismic and amblyopic monkeys compared to the normal monkey (Figure 3A, J–K). We also evaluated functional differences in RGCs using PHNR and STR, which directly reflect RGC activity (Machida, 2012). Our results showed increased functional latencies of STR and decreased amplitudes of STR in strabismic and amblyopic monkeys, as well as PHNR latency in the strabismic monkey and PHNR amplitude in the amblyopic monkey (Figure 3B, C, J–K), suggesting severely impaired visual function of the RGCs in both monkeys.

We next assessed functional differences in the retinal outer neurons, especially photoreceptors, bipolar cells, and amacrine cells, using a-wave, b-wave (Liu et al., 2018), and OPs (Ettaiche et al., 2006), respectively. Importantly, the latencies of rod-mediated bipolar cells, mixed rod-cone and mediated bipolar cells, OPs, and cone and cone-mediated bipolar cells were longer in the strabismic and amblyopic monkeys than in the normal monkey (Figure 3D–I, L). For photopic responses, the a-wave and b-wave amplitudes were decreased in the strabismic and amblyopic monkeys (Figure 3G, M), indicating that the functions of the cone and cone-mediated bipolar cells in the strabismic and amblyopic monkeys were impaired compared to the normal monkey. The amblyopic monkey also showed markedly lower amplitudes of rod responses, maximal a- and b-waves, OPs, and 10 Hz and 30 Hz flicker responses (Figure 4D–F, H, I, M), indicating that the functions of rod-mediated bipolar cells (Marmor et al., 2009), mixed rod-cone and mediated bipolar cells, amacrine cells, and ON and OFF cones (Tanimoto et al., 2015) were reduced. Thus, the visual pathway functions were impaired in both monkeys, especially visual function in the amblyopic monkey.

Natural strabismic and amblyopic monkeys exhibit abnormal impaired retinal structure

As visual neurophysiological defects may also be associated with structure, we further investigated retinal neurostructural differences among monkeys. We evaluated differences in retinal layer thickness and fovea structure by reconstructing the 3D retinal structure. Different retinal layers were visualized by OCT scanning, with dark nuclear layers interleaved with light plexiform layers and nerve fiber layer (NFL). To ensure the accuracy of different layer segmentation, we developed a semi-automatic algorithm to mark the nine segmentation lines and delineated the following retinal layers: outer segment (OS), inner segment (IS), outer nuclear layer (ONL), outer plexiform layer (OPL), inner nuclear layer (INL), inner plexiform layer (IPL), GCL, and NFL. The 3D views of retinal layers among the normal, natural strabismic, and amblyopic monkeys were then reconstructed (Figure 4A, D, G), and mean thicknesses among different layers (Figure 4B, E, H) were calculated. As the fovea contains a high density of cone neurons (Hoshino et al., 2017) and accounts for 50% of retinal output neurons (Sinha et al., 2017), we also calculated fovea scan thickness (Figure 4C, F, I). Compared with the normal monkey, the mean and fovea scan thicknesses of the total retinal layers were thinner in the retinas of the strabismic and amblyopic monkeys, especially GCL and ONL thickness (Figure 4J–K), consistent with the visual neurophysiological differences in the target retinal neurons (Figure 3). We also examined structural differences in the center fovea of the monkeys (Figures 4C, F, I, 5A), and assessed differences by building mathematical models to fit the structure (Figure 5B). The center fovea structures of the strabismic and amblyopic monkeys (Figure 5C), including area, height, maximum width, diameter, and FWHM, were smaller than those of the normal

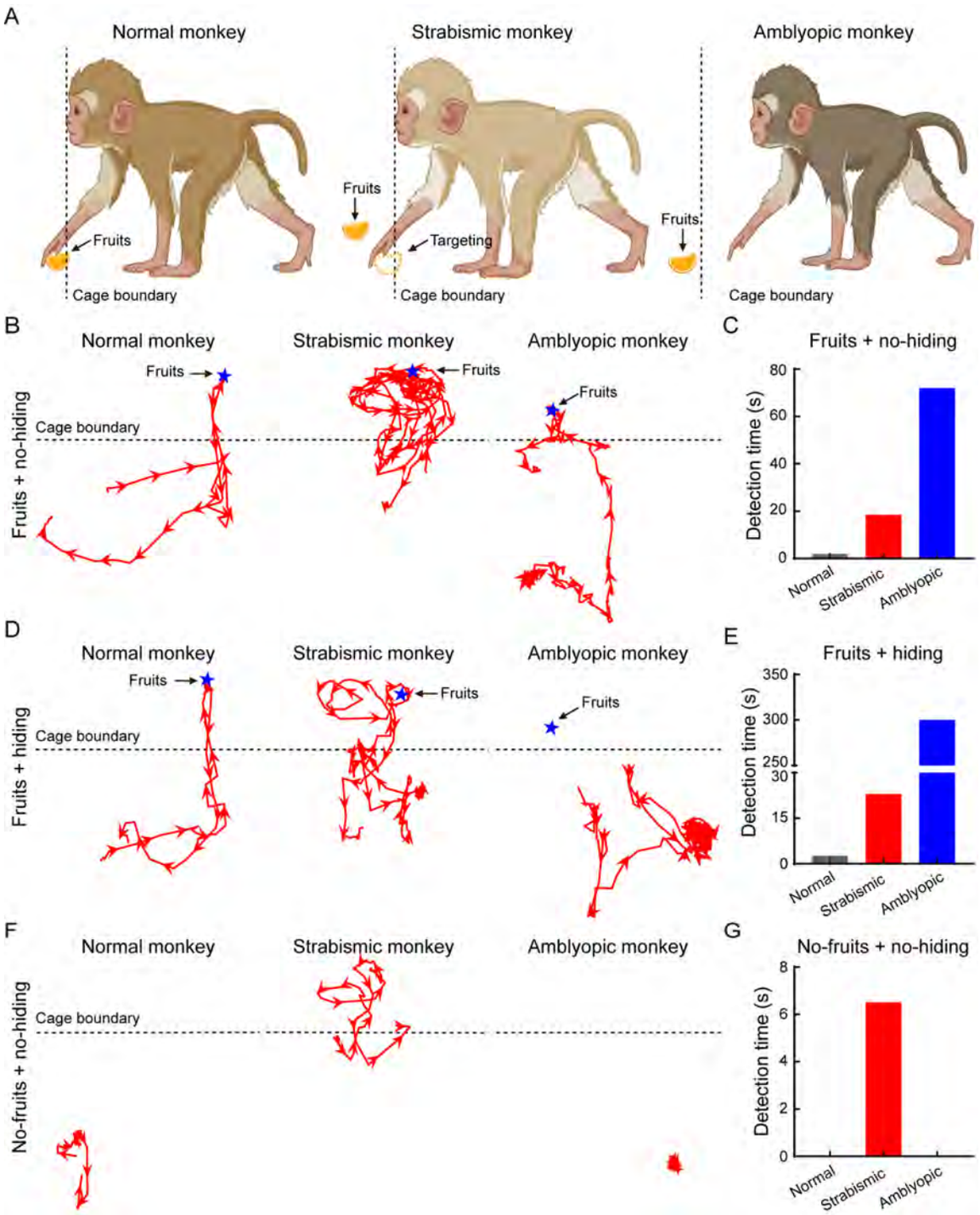

Figure 2 Natural strabismic and amblyopic monkeys show weakened visual behavioral ability

A: Schematic of targeting reward among normal (left), natural strabismic (middle), and natural amblyopic (right) monkeys. Normal monkey always directly targeted rewards, whereas natural strabismic monkey frequently deviated from the reward and natural amblyopic monkey was too timid to pick up the random reward. B, D, F: Moving trajectories (red lines) of the palm in normal (left), strabismic (middle), and amblyopic (right) monkeys. Protocols of fruits+no-hiding (B), fruits+hiding (D), and no-fruits+no-hiding (F) were performed to evaluate visual behavior differences. Outside moving trajectory of the strabismic monkey was more than that of the normal monkey. C, E, G: Detection time of normal (gray), strabismic (red), and amblyopic (blue) monkeys among different behavioral protocols. Natural strabismic monkey took longer to detect the random reward than the normal monkey in all three protocols, whereas the timid natural amblyopic monkey spent more time targeting the fixed position reward. In the fruits+hiding protocol, the natural amblyopic monkey spent more than 5 mins without obtaining the reward. Blue pentagrams, red arrows, and black dotted lines represent reward, moving direction, and cage boundary, respectively.

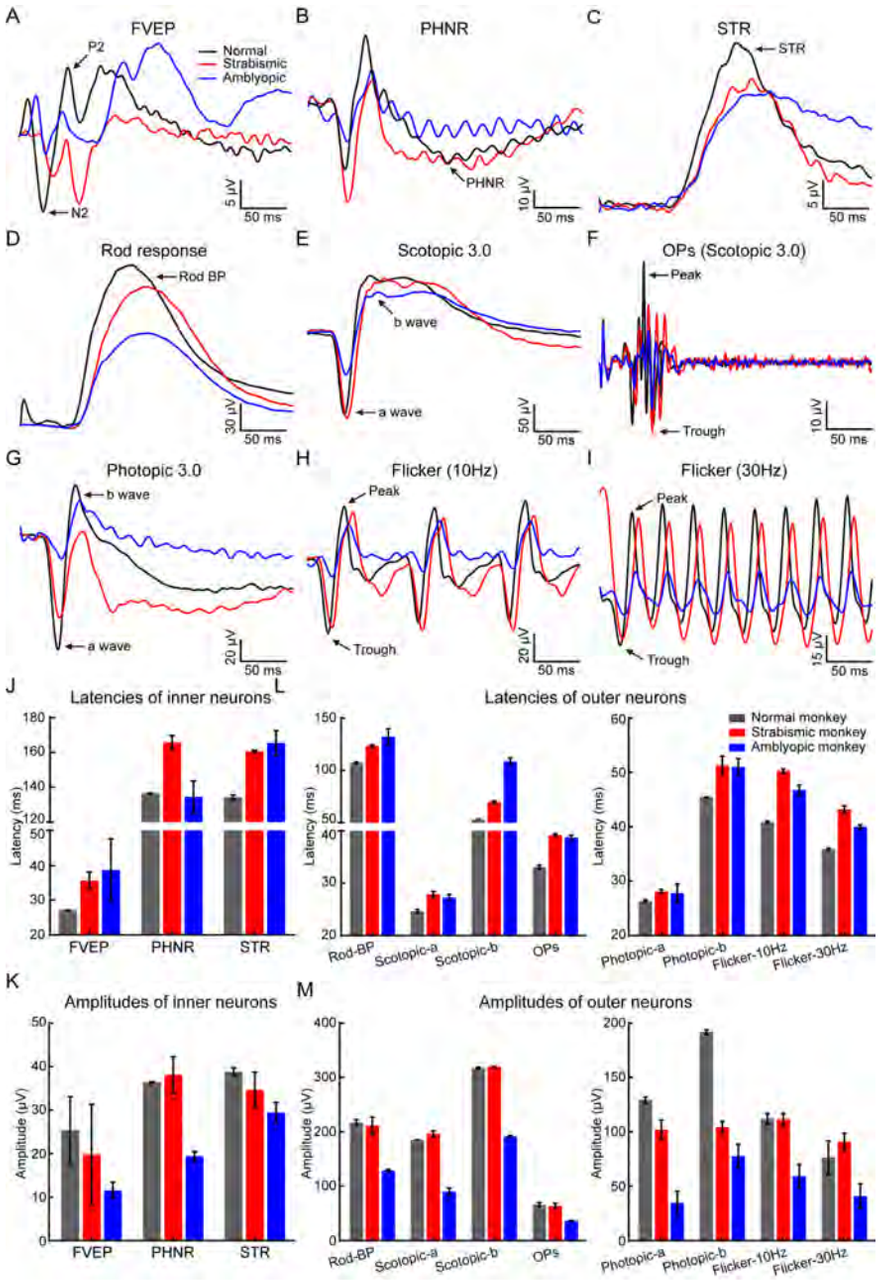

Figure 3 Natural strabismic and amblyopic monkeys exhibit weaker visual function

A: FVEP response curves of normal (black), strabismic (red), and amblyopic (blue) monkeys showing differences in functional integrity of the visual pathway, involving RGCs, optic nerve, and visual cortex. B, C: Functional differences in RGCs were directly evaluated by PHNR (B) and STR (C) curves. D: Functional differences in rod-mediated bipolar cells were evaluated by scotopic rod response curves. E, F: Scotopic maximal responses (E) and corresponding OPs (F) curves indicated functional differences in mixed rod-cone, bipolar cells, and amacrine cells, respectively. G: Functional differences in cone-pathway were shown by photopic recording. H, I: Functional differences in ON and OFF cone-pathways were revealed by 10 Hz (H) and 30 Hz (I) flicker response curves, respectively. J, K: Quantitative results of latencies and amplitudes of inner neurons for all three groups. Functional latencies of FVEP and STR in strabismic and amblyopic monkeys were longer than those in the normal monkey, whereas the FVEP and STR amplitudes were lower. Similarly, the PHNR latency in strabismic monkey was increased and the PHNR amplitude in the amblyopic monkey was decreased. L, M: Responsive latencies and amplitudes of retinal outer neurons among all three groups. Compared with the normal monkey, functional latencies of photoreceptors, cones, bipolar cells, and amacrine cells were longer in the retinas of the natural strabismic and amblyopic monkeys. Amplitudes were weaker in the natural amblyopic monkey than in the normal monkey, as was the cone-pathway in the natural strabismic monkey. Black, red, and blue represent normal, strabismic, and amblyopic monkeys, respectively, in all subfigures. FVEP, flash visual evoked potentials; PHNR, photopic negative response; STR, scotopic threshold response; BP, bipolar cell; OPs, scotopic oscillatory potentials.

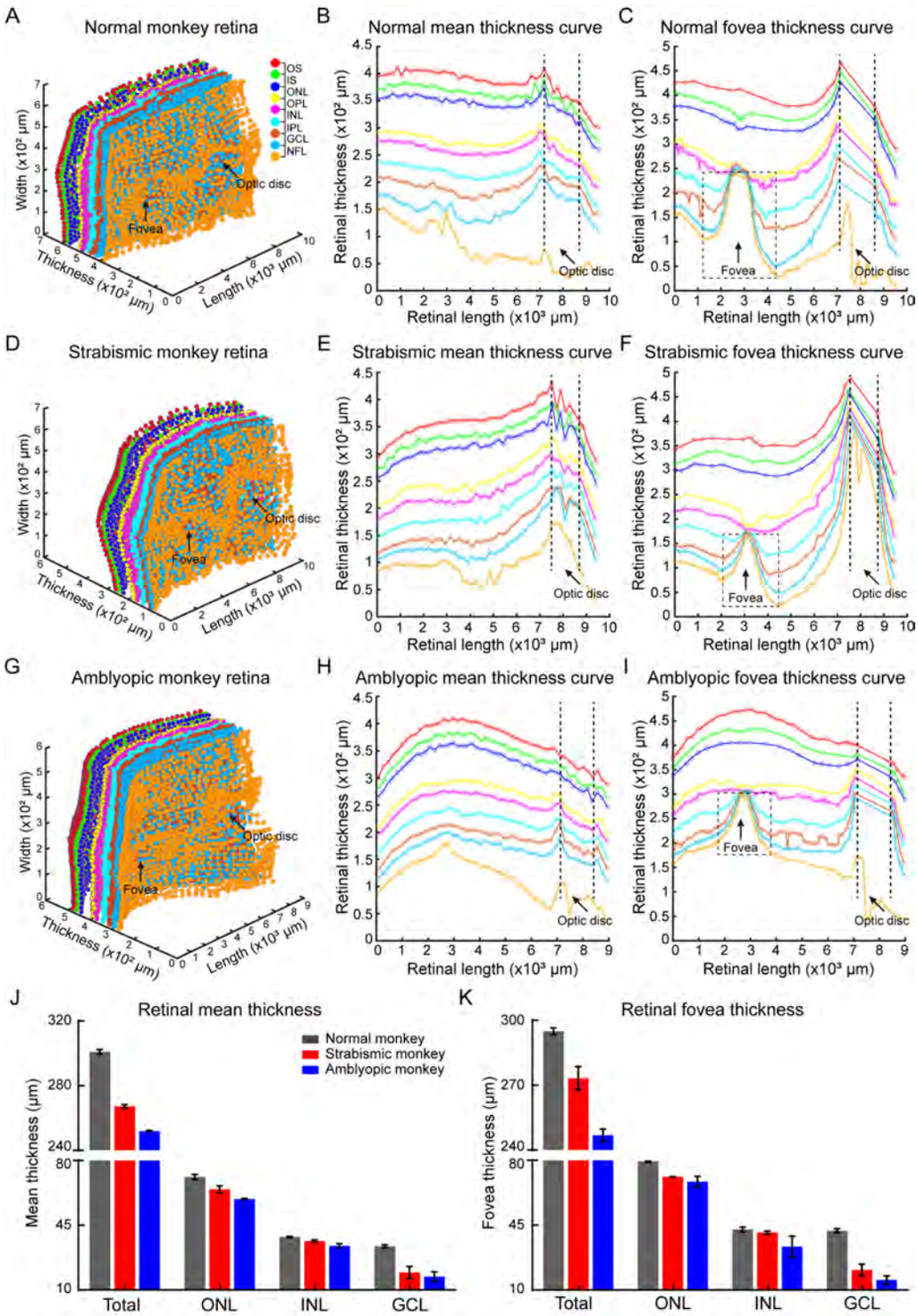

Figure 4 Natural strabismic and amblyopic monkeys show more vulnerable retinal structure

A–I: Visualization of 3D reconstruction of all retinal layers (A, D, G) and mean (B, E, H) and representative fovea (C, F, I) thickness profiles of different retinal layers among normal (A–C), natural strabismic (D–F), and amblyopic (G–I) monkeys. Hollow sizes of central fovea were smaller in natural strabismic and amblyopic monkeys than in normal monkey. J, K: Quantitative results of mean (J) and fovea (K) thickness among different retinal nuclear layers of the three groups. Mean and fovea thicknesses of total retinal layers were smaller in natural strabismic and amblyopic monkeys than in the normal monkey, as was thickness of GCL and ONL. OS, outer segment; IS, inner segment; ONL, outer nuclear layer; OPL, outer plexiform layer; INL, inner nuclear layer; IPL, inner plexiform layer; GCL, ganglion cell layer; NFL, nerve fiber layer. Black vertical dashed lines (B, C, E, F, H, I) represent optic disc boundaries. Black dotted boxes (C, F, I) indicate central fovea hollows.

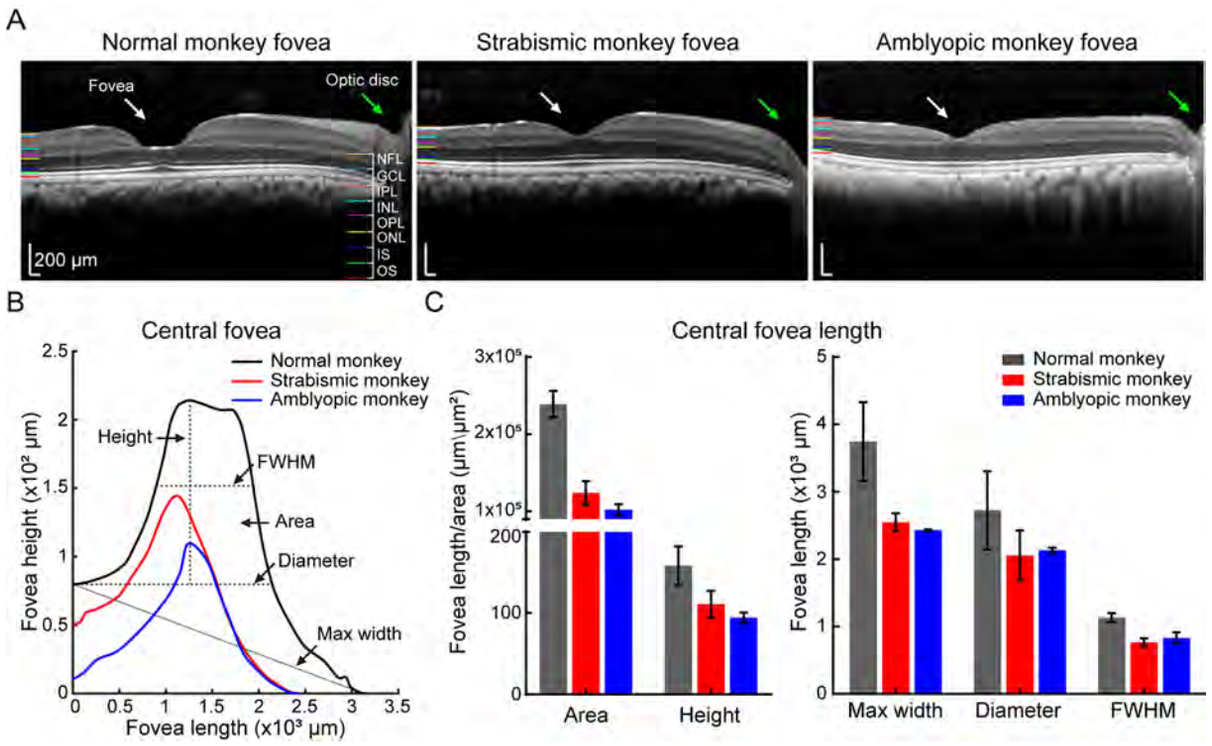

Figure 5 Natural strabismic and amblyopic monkeys show abnormal central fovea structure

A: Fovea OCT view window in normal (left), strabismic (middle), and amblyopic (right) monkeys, showing structural differences in central fovea. B: Visualization of central fovea structural reconstruction, with corresponding evaluation criteria for the three groups. C: Quantitative analysis of central fovea structural differences among the three groups. Compared with the normal monkey, fovea area, height, maximum width, diameter, and FWHM were smaller in the retina of the natural strabismic and amblyopic monkeys. White and green arrows represent fovea and optic disc, respectively. Black, red, and blue represent normal, strabismic, and amblyopic monkeys, respectively, in all subfigures.

monkey, implying that morphological variability in the fovea structure primarily resulted from abnormal foveal development (Bringmann et al., 2018). These results demonstrated that retinal structures were more susceptible in natural strabismic and amblyopic monkeys.

In addition, we also investigated differences in the fundus in the monkeys. The optic discs, where blood vessels and the optic nerve enter the eye, appeared as normal oval shapes in all groups (Figure 6A). Interestingly, the blood vessels in the eyes of the amblyopic monkey exhibited disorganization. We further calculated the CDR, which was higher in the strabismic and amblyopic monkeys than in the normal monkey (Figure 6B), consistent with functional impairment of RGCs (Figure 3). The higher CDR in the natural strabismic and amblyopic monkeys suggests more severely impaired nerve fibers.

Natural strabismic and amblyopic monkeys show closely related asymmetries in visual function and structure

With the obvious asymmetry in brain volume in the strabismic and amblyopic monkeys, we further investigated the functional and structural asymmetries in the visual pathway. Functional and structural indices were calculated to assess asymmetries based on the L/R ratio, such as FVEP and PHNR amplitudes, brain hemispherical area, GCL thickness, etc. As shown in Figure 7A, the FVEP and PHNR amplitudes in the strabismic and amblyopic monkeys were smaller in the left eye than in the right eye, indicating that the visual pathway of the left eye was more seriously injured. In the rod-pathway, rod-response amplitude was lower in the left retina of the strabismic monkey, suggesting that the function of rod-mediated bipolar cells was more severely impaired in the left retina. For photopic and flicker responses, amplitudes in the left retina were larger than those in the right retina, indicating relatively enhanced function of the cone-pathway in the left retina of the strabismic and amblyopic monkeys. The strabismic and amblyopic monkeys also showed a reduced CDR and brain hemisphere area on the right side compared with the left side, but thinner mean GCL thickness in the left retina than in the right retina (Figure 7B). Mean ONL and INL thicknesses of the left and right retinas did not differ significantly. Importantly, smaller brain hemisphere area on the right side, as well as thinner GCL thickness and larger CDR on the left side, were associated with impaired function of the left visual pathway (Figure 7A). Finally, we also assessed the functional and structural asymmetric relationships between the strabismic and amblyopic monkeys. Both functional and structural asymmetries of the strabismic monkey were significantly correlated with those of the amblyopic monkey (Figure 7C, D, $P \leq 0.01$). Taken together, our data revealed that both the natural strabismic and amblyopic monkeys exhibited consistent and correlative asymmetries in visual function and structure.

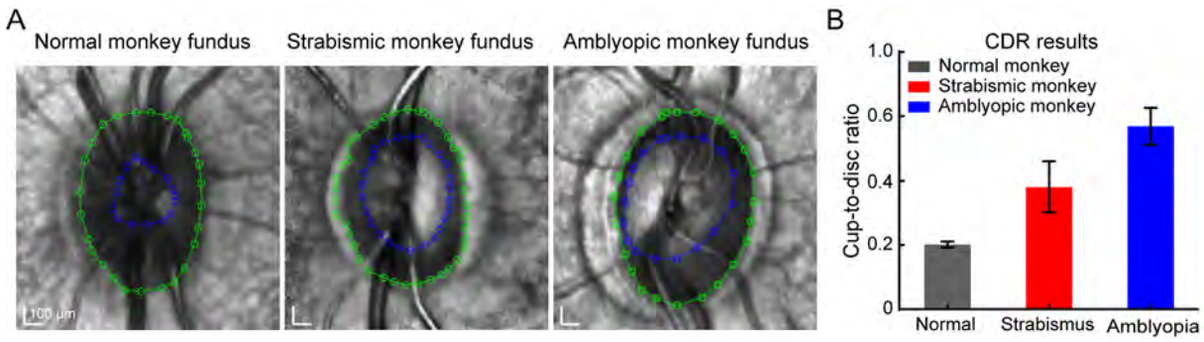

Figure 6 Natural strabismic and amblyopic monkeys exhibit higher retinal CDR

A: Size of optic disc and optic cup in normal (left), strabismic (middle), and amblyopic (right) monkeys. Diameters were calculated using an interpolation fitting method in Matlab. Green and blue lines represent optic disc and optic cup boundaries, respectively. B: Quantitative analysis of CDR in three groups. CDR was higher in the natural strabismic and amblyopic monkeys compared with the normal monkey. Black, red, and blue represent normal, strabismic, and amblyopic monkeys, respectively. CDR, cup-to-disc ratio.

Natural strabismic and amblyopic monkeys contain similar mutant genes for strabismus and amblyopia diseases

To investigate the genetic causes of natural strabismus and amblyopia in monkeys, we filtered certain mutant candidate genes using WGS, then mapped them to known strabismus- and amblyopia-associated genes. According to SnpEff annotation, only variants with high and moderate effects were considered as "impactful". We extracted several candidate genes from the strabismic and amblyopic monkeys and visualized their relationship between the two effects, respectively (Figure 8A, B). To identify enriched genes for strabismus and amblyopia, we performed DisGeNET analysis and identified gene-disease associations (Supplementary Figure S2). After extracting hereditary disease driver genes, several strabismus- and amblyopia-associated genes were successfully mapped, and their mutation rates were determined (Figure 8A, B). Both the natural strabismic and amblyopic monkeys contained some of the same strabismus- (e.g., *GDF1*, *GTF2I*, *CTDP1*, *PRSS56*, *SHH*, etc) and amblyopia-associated genes (e.g., *CHST3*, *CACNA1E*, *TWIST1*, *WDR26*, *CACNA1A*). Further network analysis of the above disease driver genes was performed to predict functional gene-gene interactions using the String database and Cytoscape. Visualization of the genetic interactions revealed a clear network for the strabismic and amblyopic monkeys (Figure 8C, D). The top three closely linked genes for the strabismic (*SHH*, *KRAS*, and *PTEN*) and amblyopic monkeys (*NOTCH1*, *GLI2*, and *SHH*) were successfully identified. In addition, network analysis of the top mutational candidate genes was performed (Supplementary Figure S3), showing that the *SHH* gene played a major role in the whole regulation network. Overall, the natural strabismic and amblyopic monkeys contained similar known mutation genes associated with strabismus and amblyopia.

DISCUSSION

This study investigated the neurological defects of strabismus and amblyopia and their relationships. We screened a natural strabismic monkey and a natural amblyopic monkey from hundreds of monkeys, as well as one human clinical strabismus case with similar disease symptoms, and comprehensively explored the brain, behavioral, visual neurophysiological, neurostructural, and genetic abnormalities. The patient and monkeys showed aberrant asymmetrical structures of the whole brain, especially an impaired visual cortex in the smaller right hemisphere. Visual behavior, function, and neurostructure of the visual pathway were impaired in the monkeys. In particular, both monkeys showed abnormal and closely related asymmetries in visual function and structure, indicating greater impairment of the left visual pathway. Certain mutant genes for strabismus and amblyopia were also identified in both monkeys. This is the first comprehensive report on asymmetrical impairment of the visual system caused by natural strabismus and amblyopia.

Visual relationships between strabismus and amblyopia

Strabismus and amblyopia are developmental ocular diseases derived from abnormal visual experiences and may be multivariate. Previous studies have shown that experimentally induced strabismus can lead to amblyopia in some monkeys (Barrett et al., 2013) and abnormalities in the orientation and/or spatial frequency maps can lead to amblyopia, which may itself lead to strabismus (Quoc & Milleret, 2014). While the cerebral cortex and lateral geniculate body are involved in strabismus and amblyopia (Al-Haddad et al., 2020; Liao et al., 2019; Quoc & Milleret, 2014; Smith III et al., 2017), evidence for direct changes in the visual pathway remains unclear. Although amblyopia is often thought to be a monocular condition, binocular abnormalities of the entire visual system in strabismus and amblyopia should also be considered. In the diagnosis and treatment of strabismus and amblyopia, binocular visual differences in the neurostructure and neurophysiology of the visual pathway are usually ignored. Consequently, the visual nervous system further deteriorates, which may cause permanent visual impairment. In the current study, we used natural strabismic and amblyopic monkeys as relevant NHP models and found marked abnormalities and asymmetries throughout the visual system. Notably, visual neurophysiology, neurostructure, behavior, and brain structure were impaired in both monkeys. Furthermore, the left retinas of both monkeys showed weaker light responses from RGCs corresponding to thinner GCL. Both rod-mediated and cone-

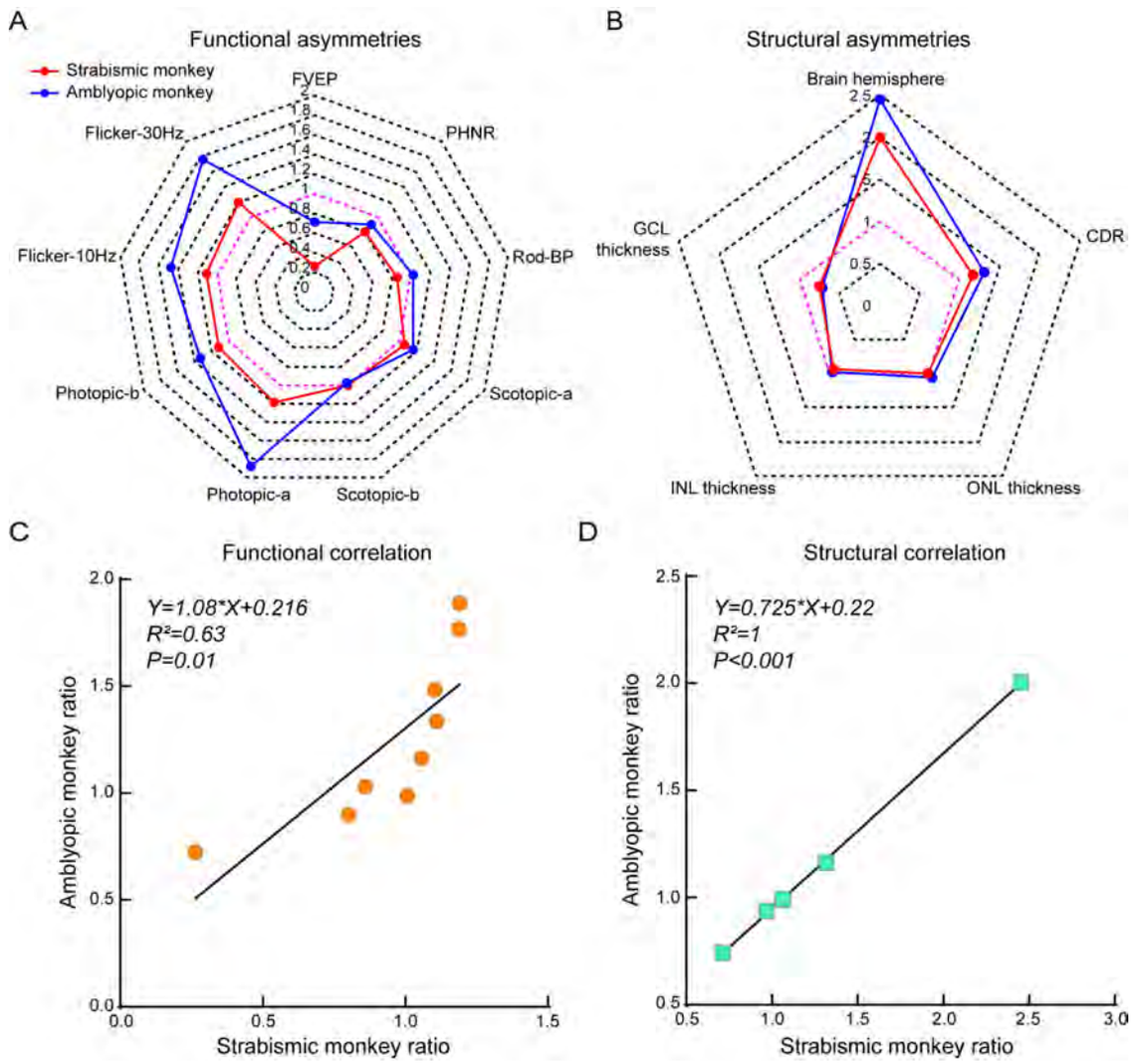

Figure 7 Natural strabismic and amblyopic monkeys show similar functional and structural asymmetries in the visual pathway

A: Visual functional asymmetries of strabismic and amblyopic monkeys based on L/R ratio of FVEP and ERG amplitudes. Functional amplitudes of FVEP and PHNR in the left retina were weaker than those in the right retina in strabismic and amblyopic monkey, whereas amplitudes of photopic and flicker responses were the opposite. B: Corresponding structural asymmetries based on L/R ratio of brain hemisphere area, CDR, GCL, INL, and ONL thickness. GCL thickness of the left retina was thinner than that of the right retina in strabismic and amblyopic monkeys, while brain hemisphere and CDR showed the opposite. C, D: Ratio scatter plots showing correlation in functional and structural asymmetries between strabismic and amblyopic monkeys. There was a significant correlation between strabismic and amblyopic monkeys in functional and structural asymmetries of the visual pathway. Red and blue lines represent L/R ratio of strabismic and amblyopic monkeys, respectively. Pink lines indicate that the ratio between the left and right sides was 1.

mediated functions were impaired in the strabismic and amblyopic monkeys compared with the control monkey, but cone function was better in the affected eye when comparing the left and right eyes. Previous studies have revealed that amblyopia and strabismus can lead to deficits in the fellow eye, and maturation of visual functions associated with the fellow eye may be disrupted along with those of the affected eye (Meier & Giaschi, 2017). Therefore, the relatively enhanced visual function of the cone-pathway in the left retina may be associated with disruption of fellow retinal maturation. We also noted signs of foveal immaturity in both monkeys, implying that foveal development may be abnormal as a result of disease progression. Similar to the strabismic monkey, there was a tendency for optic disc depression in the amblyopic monkey, as indicated by the larger CDR (Mvoulana et al., 2019). FVEP response from the left eye was also smaller, which may be due to input from the reduced RGC response or right atrophic visual cortex. Considering the visual functional and structural asymmetries, the relationship between the strabismic and amblyopic monkeys was also closely related. In brief, natural strabismus and amblyopia are visual neurological defects with pathophysiological changes from the retina to the visual cortex.

Strabismic patients with abnormal brain development or

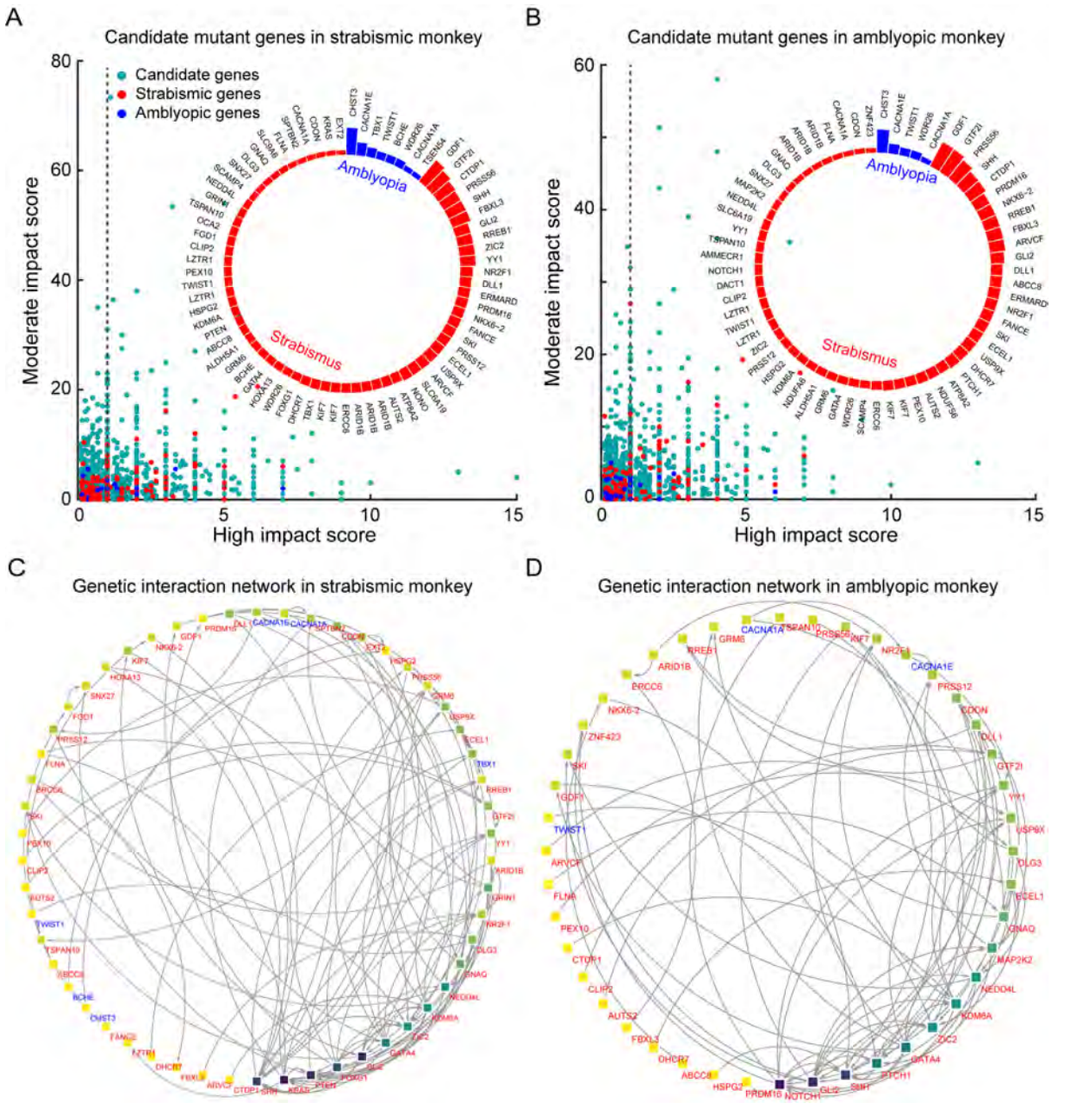

Figure 8 Natural strabismic and amblyopic monkeys contain similar known mutant genes associated with strabismus and amblyopia

A, B: Candidate mutant genes in strabismic and amblyopic monkeys revealed by WGS and annotated by SnpEff. Relationship between high and moderate effects indicated successful mapping of strabismus- and amblyopia-associated genes. Turquoise, red, and blue solid dots represent candidate, strabismus-associated, and amblyopia-associated mutant genes, respectively. Only disease-associated genes with a score above 1 were used for further analysis. Inserted circular bar chart shows distribution of degree of genetic variation among strabismus- and amblyopia-associated genes. C, D: Differences in genetic interaction networks of disease-associated genes between strabismic (C) and amblyopic (D) monkeys. Network of genes involved in strabismus and amblyopia show patterns of disease-associated genetic interactions. Nodes and edges indicate disease-associated genes and interactions between two genes, respectively, and direct interactions are shown with arrows. Darker node background indicates stronger interactions. Red and blue gene names represent strabismus- and amblyopia-associated genes, respectively.

acquired damage are most likely to have congenital cranial dysinnervation disorders (CCDDs) and paralytic/non-concomitant strabismus (Khan et al., 2014; Whitman & Engle, 2017). In contrast to CCDDs or nerve palsies, most strabismus such as congenital strabismus, accommodative strabismus, and divergent strabismus are concomitant (Quoc & Milleret, 2014). Although most strabismus cases in humans and monkeys are not accompanied by obvious organic lesions of the central and visual systems on imaging, abnormalities in the visual system can be detected by electrophysiology, functional MRI, and binocular visual function (Das, 2016; Quoc & Milleret, 2014; Tan et al., 2016; Yan et al., 2010). Abnormal

structural and functional brain impairments are also observed in human clinical cases (Chan et al., 2004; Quoc & Milleret, 2014; Shi et al., 2019; Tan et al., 2016; Wu et al., 2022; Yan et al., 2010). Similarly, we observed several abnormal impairments and asymmetries of neural activity in the visual pathway from the eye to brain, especially in the concomitant strabismic monkey and human patient. Although these may be very specific cases, we propose that the obvious brain impairment was related to strabismus or amblyopia for several reasons. First, persistent and permanent cortical changes can occur in subjects with concomitant strabismus, suggesting that disrupted neuronal circuits in the brain are associated with abnormal eye movement and visual defects, as reported in human cases of concomitant strabismus (Yan et al., 2019). Strabismus also affects the establishment of stable visual cortical circuits in primates and animals (Yan et al., 2019), and many studies have revealed alterations in the function of the visual cortex and brain connections within and between brain regions (Chan et al., 2004; Schmidt & Löwel, 2006; Zhang et al., 2005). Second, some patients with concomitant strabismus display both structural and functional brain abnormalities in neuroimaging (Shi et al., 2019; Tan et al., 2016; Wu et al., 2022; Yan et al., 2010), including decreased gray and white matter volume, abnormal microstructural alterations, and changes in brain activity. Third, strabismus can occur in patients with organic asymmetrical hemispheric lesions (Chan et al., 2004; Quoc & Milleret, 2014; Shi et al., 2019; Tusscher et al., 2018; Wang et al., 2018; Wang et al., 2021), as observed in this study. Fourth, structural and functional asymmetries of the cerebral hemispheres are also present in primates in the form of deprivation monocular amblyopia with definite corneal opacity, as reported in primates, felines, and humans (Hallum et al., 2017; Quoc et al., 2011; Xiao et al., 2007). Thus, our observations enrich the phenomenon of hemispheric asymmetrical impairment in the pathogenesis of strabismus and amblyopia.

Due to the extremely low prevalence of spontaneous strabismus and amblyopia, especially alternating concomitant exotropia, we only collected data from one clinical case and two naturally diseased monkeys with similar clinical symptoms. Thus, the present study was limited to a small sample size. Although it is not possible to determine whether all strabismic and amblyopic monkeys exhibit atrophic or pathological foci in their brains, our study proved that these natural disease cases do exist in humans and primates. Results and data may be more robust if the prevalence of natural strabismus and amblyopia was higher in monkeys, thus improving sample size. In addition, because of the marked increase in the cost of experimental monkeys, we only used one age-matched normal monkey as the control to minimize age differences. More control monkeys would facilitate comparison but would also increase ethical considerations and cost, which are the most common problems in primate research. Therefore, future studies with larger sample size are warranted to verify the present results. Nevertheless, this study provides new insights into the pathogenesis of strabismus and amblyopia, which should be of interest to ophthalmologists when treating patients with strabismus and amblyopia and when considering the functional integrity and symmetry of the visual system involving the eye and brain.

Potential pathogenesis of strabismus and amblyopia

The origins of strabismus and amblyopia remain poorly understood. Various origins of strabismus have been suggested, including early binocular vision impairment (Ghasia & Tychsen, 2014; Tychsen et al., 2008), abnormal extraocular muscles and/or innervation (Graeber et al., 2013), and abnormalities in connective tissue (Stager et al., 2013) and the brain control center that directs eye movements (Brodsky, 2011). Previous studies have shown that strabismus accounts for around 60% of amblyopia (Birch, 2013). Additional risk factors for amblyopia include developmental delay, premature birth, and small for gestational age (Gopal et al., 2019; Li et al., 2013; Spiegel et al., 2013). Which neural circuits in the visual system, if any, might be disrupted, causing strabismus and amblyopia? Considering that the neurological anomalies underlying strabismus and amblyopia appear to be located in the primary and secondary visual cortices (Barrett et al., 2013; Shooner et al., 2015; Smith III et al., 2017), our data showed that the anatomical structures of the whole brain in the natural strabismic and amblyopic monkeys were abnormal and asymmetrical, especially the atrophic visual cortex in the smaller right hemisphere. We also revealed similar mutant genes related to strabismus and amblyopia, suggesting that these disorders are closely associated. Generally, strabismus and amblyopia do not seem to be monogenic susceptible diseases (Quoc & Milleret, 2014), but more likely the interaction of multiple susceptible genes. Nevertheless, several obvious differences were also observed, such as the more disorganized brain structure in the strabismic monkey and leukoma and partial iris abnormality in the left eye of the amblyopic monkey. Taken together, strabismus and amblyopia indeed indicate multiple complex origins, especially defects and asymmetries in the visual system.

In the current study, it was difficult to distinguish whether abnormalities in the visual pathway were the cause or consequence of strabismus and amblyopia. More generally, any relevant genetic alterations during the critical period may result in varying degrees of abnormal development of neurostructures in the brain and eye. Immature neural networks may, in turn, cause strabismus or amblyopia. Given these observations, it is likely that brain structural asymmetry during critical periods of development contributes to a cascade of oculomotor and visual system abnormalities. Thus, we suggest that certain abnormal impairments and asymmetries in neural activity in the visual pathway from the eye to brain will inevitably induce strabismus and amblyopia and thereby visual defects.

SUPPLEMENTARY DATA

Supplementary data to this article can be found online.

COMPETING INTERESTS

The authors declare that they have no competing interests.

AUTHORS' CONTRIBUTIONS

S.L. and J.H.Y. designed the project. F.L., Z.H.W., W.H., R.L., Z.Y.L., L.T., J.Y.P., and X.S. performed the experiments. F.L., W.H., Z.Y.L., X.S., and J.R.W. analyzed the data. S.L., J.H.Y., F.L., Z.H.W., and W.H. wrote the paper. Y.X., Y.L.B., and Z.C.M. reviewed and edited the manuscript. All authors read and approved the final version of the manuscript.

ACKNOWLEDGEMENTS

We gratefully thank Dr Nancy George for language editing and proofreading.

REFERENCES

Al-Haddad C, Ghannam AB, El Moussawi Z, Rachid E, Ismail K, Atallah M, et al. 2020. Multifocal electroretinography in amblyopia. *Graefe's Archive for Clinical and Experimental Ophthalmology*, **258**(3): 683−691.

Barrett BT, Bradley A, Candy TR. 2013. The relationship between anisometropia and amblyopia. *Progress in Retinal and Eye Research*, **36**: 120−158.

Birch EE. 2013. Amblyopia and binocular vision. *Progress in Retinal and Eye Research*, **33**: 67−84.

Bringmann A, Syrbe S, Görner K, Kacza J, Francke M, Wiedemann P, et al. 2018. The primate fovea: structure, function and development. *Progress in Retinal and Eye Research*, **66**: 49−84.

Brodsky MC. 2011. Dissociated vertical divergence: cortical or subcortical in origin?. *Strabismus*, **19**(2): 67−68.

Burgoyne CF. 2015. The non-human primate experimental glaucoma model. *Experimental Eye Research*, **141**: 57−73.

Chan ST, Tang KW, Lam KC, Chan LK, Mendola JD, Kwong KK. 2004. Neuroanatomy of adult strabismus: a voxel-based morphometric analysis of magnetic resonance structural scans. *NeuroImage*, **22**(2): 986−994.

Cingolani P, Platts A, Wang LL, Coon M, Nguyen T, Wang L, et al. 2012. A program for annotating and predicting the effects of single nucleotide polymorphisms, SnpEff: SNPs in the genome of drosophila melanogaster strain w^{1118}; iso-2; iso-3. *Fly*, **6**(2): 80−92.

Das VE. 2016. Strabismus and the oculomotor system: insights from macaque models. *Annual Review of Vision Science*, **2**: 37−59.

Ettaiche M, Deval E, Cougnon M, Lazdunski M, Voilley N. 2006. Silencing acid-sensing ion channel 1a alters cone-mediated retinal function. *Journal of Neuroscience*, **26**(21): 5800−5809.

Fortune B, Bui BV, Morrison JC, Johnson EC, Dong J, Cepurna WO, et al. 2004. Selective ganglion cell functional loss in rats with experimental glaucoma. *Investigative Ophthalmology & Visual Science*, **45**(6): 1854−1862.

Ghasia F, Tychsen L. 2014. Horizontal and vertical optokinetic eye movements in macaque monkeys with infantile strabismus: directional bias and crosstalk. *Investigative Ophthalmology & Visual Science*, **55**(1): 265−274.

Gopal SKS, Kelkar J, Kelkar A, Pandit A. 2019. Simplified updates on the pathophysiology and recent developments in the treatment of amblyopia: a review. *Indian Journal of Ophthalmology*, **67**(9): 1392−1399.

Graeber CP, Hunter DG, Engle EC. 2013. The genetic basis of incomitant strabismus: consolidation of the current knowledge of the genetic foundations of disease. *Seminars in Ophthalmology*, **28**(5–6): 427–437.

Greenberg AE, Mohney BG, Diehl NN, Burke JP. 2007. Incidence and types of childhood esotropia: a population-based study. *Ophthalmology*, **114**(1): 170−174.

Hallum LE, Shooner C, Kumbhani RD, Kelly JG, García-Marín V, Majaj NJ, et al. 2017. Altered balance of receptive field excitation and suppression in visual cortex of amblyopic macaque monkeys. *Journal of Neuroscience*, **37**(34): 8216−8226.

Hoshino A, Ratnapriya R, Brooks MJ, Chaitankar V, Wilken MS, Zhang C, et al. 2017. Molecular anatomy of the developing human retina. *Developmental Cell*, **43**(6): 763−779.e4.

Ikeda Y, Nishiguchi KM, Miya F, Shimozawa N, Funatsu J, Nakatake S, et al. 2018. Discovery of a cynomolgus monkey family with retinitis pigmentosa. *Investigative Ophthalmology & Visual Science*, **59**(2): 826−830.

Joly O, Frankó E. 2014. Neuroimaging of amblyopia and binocular vision: a review. *Frontiers in Integrative Neuroscience*, **8**: 62.

Khan AO, Shaheen R, Alkuraya FS. 2014. The *ECEL1*-related strabismus phenotype is consistent with congenital cranial dysinnervation disorder. *Journal of American Association for Pediatric Ophthalmology and Strabismus*, **18**(4): 362−367.

Lambert WS, Carlson BJ, Ghose P, Vest VD, Yao V, Calkins DJ. 2019. Towards a microbead occlusion model of glaucoma for a non-human primate. *Scientific Reports*, **9**(1): 11572.

Lebherz C, Maguire AM, Auricchio A, Tang WX, Aleman TS, Wei ZY, et al. 2005. Nonhuman primate models for diabetic ocular neovascularization using AAV2-mediated overexpression of vascular endothelial growth factor. *Diabetes*, **54**(4): 1141−1149.

Levi DM. 2012. Prentice award lecture 2011: removing the brakes on plasticity in the amblyopic brain. *Optometry and Vision Science*, **89**(6): 827−838.

Li JR, Thompson B, Deng DM, Chan LYL, Yu MB, Hess RF. 2013. Dichoptic training enables the adult amblyopic brain to learn. *Current Biology*, **23**(8): R308−R309.

Liao N, Jiang HL, Mao GY, Li YY, Xue AQ, Lan Y, et al. 2019. Changes in macular ultrastructural morphology in unilateral anisometropic amblyopia. *American Journal of Translational Research*, **11**(8): 5086−5095.

Liu F, Liu XB, Zhou YM, Yu YK, Wang K, Zhou ZQ, et al. 2021. Wolfberry-derived zeaxanthin dipalmitate delays retinal degeneration in a mouse model of retinitis pigmentosa through modulating STAT3, CCL2 and MAPK pathways. *Journal of Neurochemistry*, **158**(5): 1131−1150.

Liu F, Zhang J, Xiang ZQ, Xu D, So KF, Vardi N, et al. 2018. Lycium barbarum polysaccharides protect retina in rd1 mice during photoreceptor degeneration. *Investigative Ophthalmology & Visual Science*, **59**(1): 597−611.

Machida S. 2012. Clinical applications of the photopic negative response to optic nerve and retinal diseases. *Journal of Ophthalmology*, **2012**: 397178.

MacLachlan TK, Lukason M, Collins M, Munger R, Isenberger E, Rogers C, et al. 2011. Preclinical safety evaluation of AAV2-sFLT01- a gene therapy for age-related macular degeneration. *Molecular Therapy*, **19**(2): 326−334.

Marmor MF, Fulton AB, Holder GE, Miyake Y, Brigell M, Bach M. 2009. ISCEV standard for full-field clinical electroretinography (2008 update). *Documenta Ophthalmologica*, **118**(1): 69−77.

Meier K, Giaschi D. 2017. Unilateral amblyopia affects two eyes: fellow eye deficits in amblyopia. *Investigative Ophthalmology & Visual Science*, **58**(3): 1779−1800.

Mendola JD, Lam J, Rosenstein M, Lewis LB, Shmuel A. 2018. Partial correlation analysis reveals abnormal retinotopically organized functional

connectivity of visual areas in amblyopia. *NeuroImage:Clinical*, **18**: 192−201.

Moshiri A, Chen R, Kim S, Harris RA, Li YM, Raveendran M, et al. 2019. A nonhuman primate model of inherited retinal disease. *The Journal of Clinical Investigation*, **129**(2): 863−874.

Mvoulana A, Kachouri R, Akil M. 2019. Fully automated method for glaucoma screening using robust optic nerve head detection and unsupervised segmentation based cup-to-disc ratio computation in retinal fundus images. *Computerized Medical Imaging and Graphics*, **77**: 101643.

Odom JV, Bach M, Brigell M, Holder GE, McCulloch DL, Mizota A, et al. 2016. ISCEV standard for clinical visual evoked potentials: (2016 update). *Documenta Ophthalmologica*, **133**(1): 1−9.

Picaud S, Dalkara D, Marazova K, Goureau O, Roska B, Sahel JA. 2019. The primate model for understanding and restoring vision. *Proceedings of the National Academy of Sciences of the United States of America*, **116**(52): 26280−26287.

Piñero J, Queralt-Rosinach N, Bravo À, Deu-Pons J, Bauer-Mehren A, Baron M, et al. 2015. DisGeNET: a discovery platform for the dynamical exploration of human diseases and their genes. *Database (Oxford)*, **2015**: bav028.

Quoc EB, Milleret C. 2014. Origins of strabismus and loss of binocular vision. *Frontiers in Integrative Neuroscience*, **8**: 71.

Quoc EB, Ribot J, Quenech'Du N, Doutremer S, Lebas N, Grantyn A, et al. 2011. Asymmetrical interhemispheric connections develop in cat visual cortex after early unilateral convergent strabismus: anatomy, physiology, and mechanisms. *Frontiers in Neuroanatomy*, **5**: 68.

Rangaswamy NV, Shirato S, Kaneko M, Digby BI, Robson JG, Frishman LJ. 2007. Effects of spectral characteristics of ganzfeld stimuli on the photopic negative response (PhNR) of the ERG. *Investigative Ophthalmology & Visual Science*, **48**(10): 4818−4828.

Schmidt KF, Löwel S. 2006. The layout of functional maps in area 18 of strabismic cats. *Neuroscience*, **141**(3): 1525−1531.

Scholl B, Tan AYY, Priebe NJ. 2013. Strabismus disrupts binocular synaptic integration in primary visual cortex. *Journal of Neuroscience*, **33**(43): 17108−17122.

Shi HM, Wang YM, Liu XM, Xia L, Chen Y, Lu QL, et al. 2019. Cortical alterations by the abnormal visual experience beyond the critical period: a resting-state fMRI study on constant exotropia. *Current Eye Research*, **44**(12): 1386−1392.

Shooner C, Hallum LE, Kumbhani RD, Ziemba CM, Garcia-Marin V, Kelly JG, et al. 2015. Population representation of visual information in areas V1 and V2 of amblyopic macaques. *Vision Research*, **114**: 56−67.

Sinha R, Hoon M, Baudin J, Okawa H, Wong ROL, Rieke F. 2017. Cellular and circuit mechanisms shaping the perceptual properties of the primate fovea. *Cell*, **168**(3): 413−426.e12.

Smith III EL, Hung LF, Arumugam B, Wensveen JM, Chino YM, Harwerth RS. 2017. Observations on the relationship between anisometropia, amblyopia and strabismus. *Vision Research*, **134**: 26−42.

Spiegel DP, Li JR, Hess RF, Byblow WD, Deng DM, Yu MB, et al. 2013. Transcranial direct current stimulation enhances recovery of stereopsis in adults with amblyopia. *Neurotherapeutics*, **10**(4): 831−839.

Stager D Jr, Mcloon LK, Felius J. 2013. Postulating a role for connective tissue elements in inferior oblique muscle overaction (an american ophthalmological society thesis). *Transactions of the American Ophthalmological Society*, **111**: 119−132.

Tan G, Huang X, Zhang Y, Wu AH, Zhong YL, Wu K, et al. 2016. A functional MRI study of altered spontaneous brain activity pattern in patients with congenital comitant strabismus using amplitude of low-frequency fluctuation. *Neuropsychiatric Disease and Treatment*, **12**: 1243−1250.

Tanimoto N, Sothilingam V, Kondo M, Biel M, Humphries P, Seeliger MW. 2015. Electroretinographic assessment of rod- and cone-mediated bipolar cell pathways using flicker stimuli in mice. *Scientific Reports*, **5**: 10731.

Tusscher MPMT, Houtman AC, De Mey J, Van Schuerbeek P. 2018. Cortical visual connections via the corpus callosum are asymmetrical in human infantile esotropia. *Strabismus*, **26**(1): 22−27.

Tychsen L, Richards M, Wong AMF, Demer J, Bradley D, Burkhalter A, et al. 2008. Decorrelation of cerebral visual inputs as the sufficient cause of infantile esotropia. *American Orthoptic Journal*, **58**(1): 60−69.

Wang SF, Kowal TJ, Ning K, Koo EB, Wu AY, Mahajan VB, et al. 2018. Review of ocular manifestations of joubert syndrome. *Genes*, **9**(12): 605.

Wang ZH, Zhu BB, Fu LC, Yan JH. 2021. Etiology and clinical features of diplopia in south china: analysis of 303 cases. *Frontiers in Neurology*, **12**: 805253.

Whitman MC, Engle EC. 2017. Ocular congenital cranial dysinnervation disorders (CCDDs): insights into axon growth and guidance. *Human Molecular Genetics*, **26**(R1): R37−R44.

Wong AMF. 2012. New concepts concerning the neural mechanisms of amblyopia and their clinical implications. *Canadian Journal of Ophthalmology*, **47**(5): 399−409.

Wong EH, Levi DM, McGraw PV. 2005. Spatial interactions reveal inhibitory cortical networks in human amblyopia. *Vision Research*, **45**(21): 2810−2819.

Wu Q, Guo W, Hu H, Li R, Zhu H, Chen XX, et al. 2022. Altered spontaneous brain activity in patients with comitant exotropia before and after surgery: a resting-state fMRI study. *Experimental Eye Research*, **222**: 109161.

Xiao JX, Xie S, Ye JT, Liu HH, Gan XL, Gong GL, et al. 2007. Detection of abnormal visual cortex in children with amblyopia by voxel-based morphometry. *American Journal of Ophthalmology*, **143**(3): 489−493.

Yan XH, Lin XM, Wang QF, Zhang YC, Chen YM, Song SJ, et al. 2010. Dorsal visual pathway changes in patients with comitant extropia. *PLoS One*, **5**(6): e10931.

Yan XH, Wang Y, Xu LJ, Liu Y, Song SJ, Ding K, et al. 2019. Altered functional connectivity of the primary visual cortex in adult comitant strabismus: a resting-state functional MRI study. *Current Eye Research*, **44**(3): 316−323.

Ye XC, Pegado V, Patel MS, Wasserman WW. 2014. Strabismus genetics across a spectrum of eye misalignment disorders. *Clinical Genetics*, **86**(2): 103−111.

Zhang B, Bi H, Sakai E, Maruko I, Zheng JH, Smith III EL, et al. 2005. Rapid plasticity of binocular connections in developing monkey visual cortex (V1). *Proceedings of the National Academy of Sciences of the United States of America*, **102**(25): 9026−9031.

Zhang TY, Xie SY, Liu YC, Xue CH, Zhang W. 2021. Effect of amblyopia treatment on macular microvasculature in children with anisometropic amblyopia using optical coherence tomographic angiography. *Scientific Reports*, **11**(1): 39.